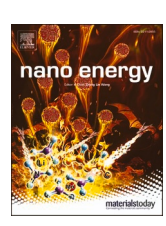
Contents lists available at ScienceDirect

Nano Energy

journal homepage: www.elsevier.com/locate/nanoen





Synthesis of color tunable piezoelectric nanogenerators using CsPbX₃ perovskite nanocrystals embedded in poly(D,L-lactide) membranes

Sk Shamim Hasan Abir ^{a,b}, Julio E. Trevino ^b, Bhupendra B. Srivastava ^c, Muhtasim Ul Karim Sadaf ^{a,c}, Julia I. Salas ^{a,b}, Karen Lozano ^{b,d,*}, Mohammed Jasim Uddin ^{a,c,**}

- ^a Photonics and Energy Research Laboratory, University of Texas Rio Grande Valley, Edinburg, TX 78539, United States
- b Department of Mechanical Engineering, University of Texas Rio Grande Valley, Edinburg, TX 78539, United States
- Department of Chemistry, University of Texas Rio Grande Valley, Edinburg, TX 78539, United States
- d Center for Nanotechnology, University of Texas Rio Grande Valley, Edinburg, TX 78539, United States

ARTICLE INFO

Keywords: Poly (D L-lactide) Perovskite nanocrystals Photoluminescence Encapsulation Piezoelectric nanogenerator

ABSTRACT

In recent years, inorganic perovskite materials have emerged as a great potential in optoelectronic and flexible nanogenerator applications. In this study, we have synthesized blue to green tunable photoluminescent (PL) inorganic CsPbX3 (X-Cl/Br) perovskite nanocrystals (NCs) utilizing a heat treatment process at a temperature of 150 °C. The purity of the NC's luminescence was analyzed utilizing PL spectroscopy and the pristine blue and green emissions were observed at a 365 nm wavelength under ultraviolet light. Furthermore, the NCs were embedded in a poly(D,L-lactide) (PDLLA) polymer matrix to fabricate flexible blue and green luminous CsPbX3-PDLLA piezoelectric nanogenerators (CPX-PDLLA PENGs). The Fourier-transform infrared spectroscopy characterization of both CPX-PDLLA PENG devices further revealed that perovskite NCs were successfully encapsulated by the PDLLA polymer matrix. The fabricated perovskite based PENGs were tested by hand tapping motion at a 240 beats per minute load frequency to explore the alternating current electrical outputs. The results illustrated that the maximum open circuit voltage and short circuit current obtained for the green PL NCs (g-CPX NCs) incorporated PENG were 1.69 and 1.42 times higher, respectively, in contrast to the blue PL NCs (b-CPX NCs) incorporated PENG. In addition, both b-CPX and g-CPX PDLLA PENGs were tested against a range of resistance and the maximum power output obtained was ~335.44 and ~797.22 µW respectively with an active contact area of 31.67 cm² for all PENGs. The developed flexible g-CPX PDLLA PENG was able to light up 50 commercial light emitting diodes (1.5 V each) indicating the vast promising applications of the PDLLA-CPX PENG as a soft high-performance self-chargeable device.

1. Introduction

Energy harvesting is the process of extracting, converting, and storing energy from environmental sources. Energy harvesting can be achieved by modulating different variables such as: pressure, vibration, motion, and temperature. Energy harvesting has sparked interest in developing new materials to establish more alternatives for the use of fossil fuels [1–3]. Among these alternatives piezoelectricity is one of the most extensively researched. Piezoelectricity is the production of electrical charges in a material or system by an applied mechanical stress

and vice versa [4,5]. Different mechanical stresses that can produce piezoelectricity include human movement, pressure, wind, rain, etc. In recent years, piezoelectric nanogenerators (PENGs) have gained rapid interest due to their potential to convert weak and irregular mechanical energy to electrical energy from the environment [6,7]. PENGs have also become attractive as an alternative to traditional batteries for low electrical power portable devices and microelectronic devices. There are many factors that affect the performance of PENGs, but the main goal of PENGs is to increase its flexibility and voltage/current output. To increase the flexibility and voltage/current output of PENGs, several

E-mail addresses: karen.lozano@utrgv.edu (K. Lozano), mohammed.uddin@utrgv.edu (M.J. Uddin).

^{*} Correspondence to: Center for Nanotechnology, Department of Mechanical Engineering, University of Texas Rio Grande Valley, Edinburg, TX 78539, United States.

^{**} Correspondence to: Photonics and Energy Research Laboratory, Department of Chemistry, University of Texas Rio Grande Valley, Edinburg, TX 78539, United States.

materials and material combinations can be utilized such as: inorganic/organic materials, chemical doping of piezoelectric materials, compatible substrates, and composite thin film materials [6,8].

Various materials including polymers [9,10], semiconductors [11, 12] and ceramics [13,14] have been utilized to develop PENGs [7,8]. Among these materials, ceramic perovskite materials are well known for their exceptional piezoelectric properties to fabricate PENGs [15,16]. However, ceramic perovskite materials are limited because of their brittleness due to their processibility. To increase the ductility of ceramic perovskite materials, polymers are introduced to provide a reinforcement for the inorganic/organic composite material [17,18]. Halide perovskites (HPs) have been utilized for their extraordinary photovoltaic and optoelectronic properties [19–21]. HPs are extremely sensitive to environmental stimuli such as pressure and temperature. Pressure and temperature cause the dipole oscillation in HPs leading to the creation of a potential difference producing electricity [15].

Ever since the first development of the PENG in 2006 by Wang et al. utilizing zinc oxide (ZnO) nanowires, different materials have been utilized to create efficient PENGs as an alternative for sustainable electrical energy [22]. For example Ding et al. fabricated a PENG consisted of formamidinium lead halide perovskite (FAPbBr₃) nanoparticles and a polydimethylsiloxane (PDMS) polymer matrix [17]. The PENG exhibited a piezoelectric output voltage of 8.5 V and current density of 3.8 μ A cm⁻² under periodically vertical compression and release. Yoon et al. applied CH3NH3PbI3 (MAPbI3) perovskite thin films to fluorine doped SnO₂ (FTO)/glass and Au/Ti/polyethylene terephthalate (PET) substrates [16]. The thin film PENGs reached a piezoelectric output voltage of 2.7 V and current density of 140 nA cm⁻². Ding et al. also fabricated a PENG consisted of FAPbBr3 nanoparticles and a poly(vinylidene fluoride) (PVDF) polymer matrix [23]. This PENG exhibited a piezoelectric output voltage of 30 V and current density of 6.2 μ A cm⁻². The PENG showed the highest outputs for voltage and current density for organic-inorganic lead halide perovskite material based PENGs.

In particular, cesium lead halide (CsPbX3, X = Cl, Br, and I) perovskites have emerged as potential semiconductor materials for various applications including solar cells [24], lasers [25], light-emitting diodes (LEDs) [26], photocatalysis [27], photodetectors [28], and visible light communication devices [29]. These materials have shown potential to become alternatives for II-VI, III-V, and IV-VI quantum dots (QDs) as the next generation of display and lighting materials because of their high quantum yield (QY), tunable wide color gamut photoluminescence, high color purity, high absorption coefficient, crystal structure, high defect tolerance, etc. [19,21,30,31]. Furthermore, CsPbX₃ perovskites have unique dielectric properties and an ideal dielectric constant promoting piezoelectric behavior [21]. CsPbX₃ perovskites have a cubic structure which also allows the unit cell to deform into various ferroelectrically active non-cubic phases [18]. The piezoelectric behavior can also be attributed to the intrinsically high polarizability caused by ionic substitution, dipolar or hopping contributions of polarons due to the non-centrosymmetric crystal structure of $[PbX_6]^{4-}$ [21]. Moreover, Mondal et al. showed that inclusion of 5 wt% of CsPbBr3 rods in ferroelectric polymers like poly (vinylidene fluoride) (PVDF) nanofiber matrix not only increased the desired electroactive β -phase (electroactive β phase in PVDF > 90 %) formation, but also enhanced overall crystallinity and dielectric permittivity in the hybrid composite yielding a maximum 120 V_{oc} and 35 $\mu A I_{sc}$ with a power output of 4.24 mW [32]. The randomly oriented CsPbBr₃ rods in the PVDF fiber matrix improved the localized electric field and domain mobility at the localized stress points. This is attributed to improved overall polarization of the fiber composite [32,33]. Furthermore, Mondal et al. demonstrates that a 3 wt % loading of CsPbCl3 nanocrystals in PVDF nanofibers facilitates an increment of over 86 % of electroactive β phase in PVDF owing to the interfacial surface charge interaction of CsPbCl₃ and -CH₂- and -CF₂dipoles of the PVDF chain [34]. An instantaneous output voltage of 168 V and peak-to-peak output current of 2 μA by hand hammering resulted from the hybrid composite.

Nevertheless, the intrinsic instability of CsPbX₃ perovskites associated with their poor stability against moisture, light, and temperature presents a challenge to develop CsPbX3 perovskite PENGs [35,36]. To overcome these issues, many synthetic strategies such as ultrasonication [37], chemical vapor deposition [38], ball-milling synthesis [39], microwave-assistance [40], including numerous synthetic alterations in hot injection technique [41] have been attempted to synthesize CsPbX₃ nanocrystals (NCs). However, the imbalance in stoichiometric equilibrium between cations and anions are affected by the inert atmosphere and high temperature associated with large-scale production of CsPbX3 NCs [42,43]. Another method utilized to protect CsPbX₃ NCs is the encapsulation within protective matrices, which prevents NCs from segregation as well as safeguard them from thermal and environmental instability [19,44]. A gamut of protective methods such as atomic layer deposition, spin coating, protective coating, nanoparticle coating, polymer matrix methods, and polymer blend techniques have been applied to enhance the stability of CsPbX3 NCs [45,46]. However, reported studies still face significant challenges to ensure a uniform distribution of NCs in matrices, a low production rate, monotonous post treatment to prepare the perovskite materials, etc. [19].

Recently, encapsulation of perovskite NCs in a polymer matrix has drawn significant attention as polymer matrices besides aiding in preventing agglomeration also provide mechanical and chemical stability to the NCs. Furthermore, polymer matrices offer processability towards thin films and microsphere structures among other systems. In this study, we have successfully synthesized blue and green photoluminescent CsPb(Br/Cl)₃ perovskite NCs embedded in a poly(D,L-lactide) (PDLLA) polymer matrix. PDLLA was utilized because of its biodegradable, mechanical, moisture resistance, flexible processibility properties [47]. In addition, polylactide based polymer composite/fibers offer enhanced piezoelectric performance which can be applied to electronic skin sensor and energy harvesting applications [48–50]. Zhao et al. showed that the piezoelectric response of poly (L-Lactic) acid (PLLA) fibers results from the C=O dipole polymer chains [49]. The C=O function group of PLLA fibers is associated with the α phase generally located around the 10_3 helical structure whereas the β phase is located at the 3₁ helical structure [49,50]. These two main polymer chains generally arrange in an antiparallel formation relative to each other, so in normal conditions the PLLA doesn't show piezoelectric properties [50,51]. However, under shear stress or under a strong electric field, the polymer chains twist and eventually the C=O dipole components orient along the carbon main chain direction and make them parallel to each other [48]. This results in a piezoelectric response along the fiber direction [48,49]. In addition, the β crystal structure results from the stretching of the PLLA material correlating to the thermal stability and piezoelectric response as presented by Gong and Oumghar et al. [48,52].

Here, in this investigation, developed PENGs were subjected to nano/microscopic morphology, infrared spectroscopy, and photo-luminescence spectroscopy analysis to inspect the NC's structure, shape, size, distribution, photophysical properties, compositional stretching of different bonds present in the perovskite NCs and its associated CsPbX₃-PDLLA piezoelectric films. In addition, the effect of encapsulated CsPbX₃NCs on the piezoelectric performance of the fabricated polymeric CsPbX₃-PDLLA PENGs were also investigated under a range of hand tapping motions to illustrate alternating electrical (AC) output (open circuit voltage and short circuit current). Furthermore, the PENGs were also tested against various capacitors and resistive loads to explore the applicability of synthesized CsPbX₃-PDLLA PENGs for the prospective charging of small electronic devices and lighting commercial light emitting diodes (LEDs) within a short period of time.

2. Experimental

2.1. Materials

Poly (D,L- lactide) (PDLLA) with MW = 160 kgmol^{-1} was purchased from NatureWorks LLC (Ingeo 6362D). Lead (II) bromide (PbBr₂, ≥ 98 %), cesium chloride (CsCl, 99.99%), toluene (C₇H₈, ≥ 99 %), N,N, dimethylformamide (DMF, ≥ 99.7 %) and chloroform (CHCl₃, ≥ 99 %) were all provided by Fisher Scientific. Oleyl amine (OA, 70%) and oleic acid (OLA, 90%) obtained from Sigma Aldrich. All materials were utilized as received without any further purification.

2.2. Preparation of CsPb(Cl/Br)3 NCs encapsulated PDLLA film

The blue and green CsPb(Cl/Br)₃ NCs synthesis technique was addressed in our previous work [19]. The synthesized NCs will be known as b-CPX and g-CPX NCs. To prepare the PDLLA polymer solution, PDLLA was first added to a CsPb(Cl/Br)₃ NC embedded chloroform solution in a 20 mL glass vial to make 13 wt% polymer solutions. The solution was then stirred with a magnetic stirrer for 12 hr at 800 rpm to ensure complete dissolution. Then, the solution was poured into a petri dish and kept in the oven at 60 °C for 6 hrs to obtain a PDLLA polymer film by removing all the solvent from the system. The final NCs encapsulated polymer films are abbreviated as b-CPX PDLLA and g-CPX PDLLA films. Fig. 1 illustrates the synthesis of b-CPX NCs, g-CPX NCs, b-CPX PDLLA film, g-CPX PDLLA film, the encapsulation of NCs in the PDLLA film and their respective bright blue and green photo luminescent emission under ultraviolet (UV) irradiation at 365 nm wavelength.

2.3. Fabrication of CPX PDLLA PENG

The CPX PDLLA films were removed from the petri dish and cut into circular shapes with a diameter of 6.35 cm. To properly create the PENG, commercially available copper (Cu) tape was attached on both sides of the film to work as electrodes. All the electrical tests were done in ambient conditions.

2.4. Characterization

The synthesized b-CPX and g-CPX NCs were analyzed using a Bruker

D8 Advance X-ray diffractometer (XRD) with Cu K α 1 radiation ($\lambda=0.15406$ nm). The obtained XRD data was collected using a scanning mode of 2θ with a scanning step size of 0.04° and a scanning rate of 2.0° min $^{-1}$. The morphology of the CPX-PDLLA films were characterized by using a field emission scanning electron microscope (FESEM) with an acceleration voltage of 1.0 kV (Sigma VP, Carl Zeiss, Jena, Germany). The fourier Transform Infrared (FTIR) Spectra of the NCs and NC encapsulated piezoelectric films were performed by using a 133 VERTEX 70 v FTIR Spectrometer (Bruker). The transmittance data of the NCs and polymer films were recorded from a range of 450 cm $^{-1}$ to 4000 cm $^{-1}$ wavelengths. Photoluminescent (PL) spectroscopy measurements were carried out by using an Edinburgh Instrument FLS 980 spectrometer with a steady state xenon lamp source. The PL intensity data was recorded from a range of 400–600 nm wavelengths.

2.5. Measuring of electrical output

The open circuit output voltage of the b-CPX and g-CPX PDLLA PENG was measured by a Tektronix TDS1001B digital oscilloscope while the short-circuit current was measured by a Stanford Research Systems SR570 current preamplifier connected to the oscilloscope.

3. Results and discussion

Transmission electron microscopy (TEM) morphology of the CPX perovskite NCs is illustrated in Fig. 2a-d. Fig. 2a and b represent the b-CPX and Fig. 2c and d represent the g-CPX NCs at different magnifications. It is shown in Fig. 2a and b that the b-CPX NCs are monodispersed with a diameter of 10-20 nm with a spherical shape. The stabilization of uncombined and separated natural b-CPX NCs in chloroform can be elucidated by coulombic interactions among the b-CPX perovskite nanocrystals overcoming the van der Waals forces [19]. A similar trend of the morphological structure was also observed for g-CPX NCs with a diameter increase of 20-30 nm. The distinctive aggregation of the NCs can be ascribed to thermal treatment at 150 °C. Fig. 2g illustrates the XRD patterns of the perovskite b-CPX and g-CPX NCs and their corresponding b-CPX and g-CPX PDLLA polymer composite films. The synthesized b-CPX NCs and their corresponding peaks match with the cubic CsPbBr₃ crystal structure according to the CPDS number 54-0752 [19, 53] indicating the same structure as CsPbBr₃. However, the 2θ angle

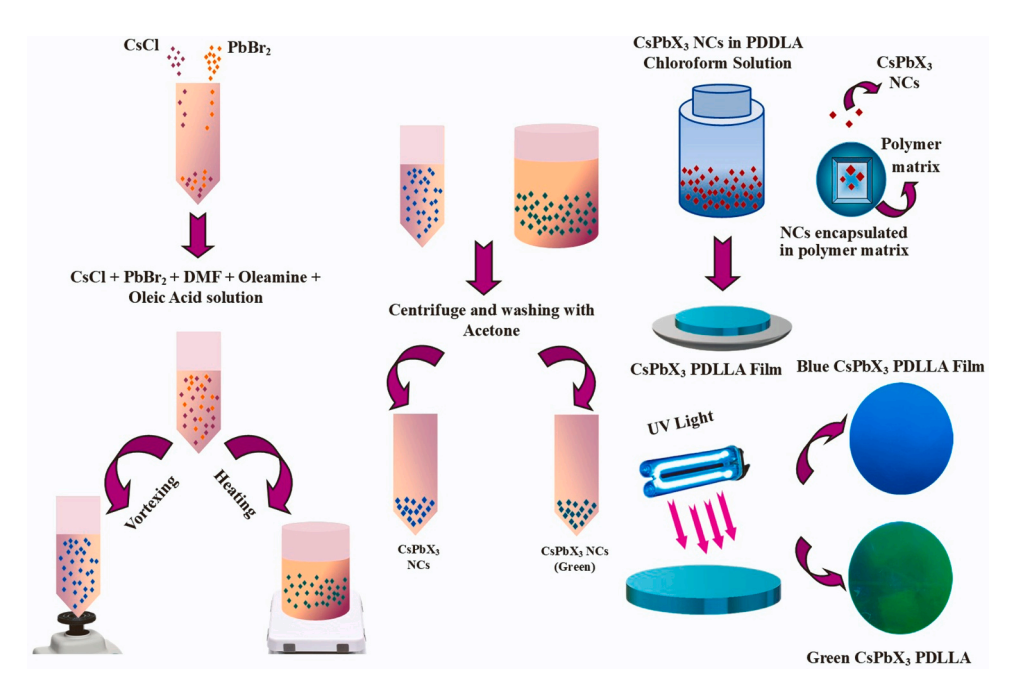


Fig. 1. Schematic of synthesis mechanism of photo luminous b-CPX, g-CPX NCs and b-CPX PDLLA, g-CPX PDLLA film.

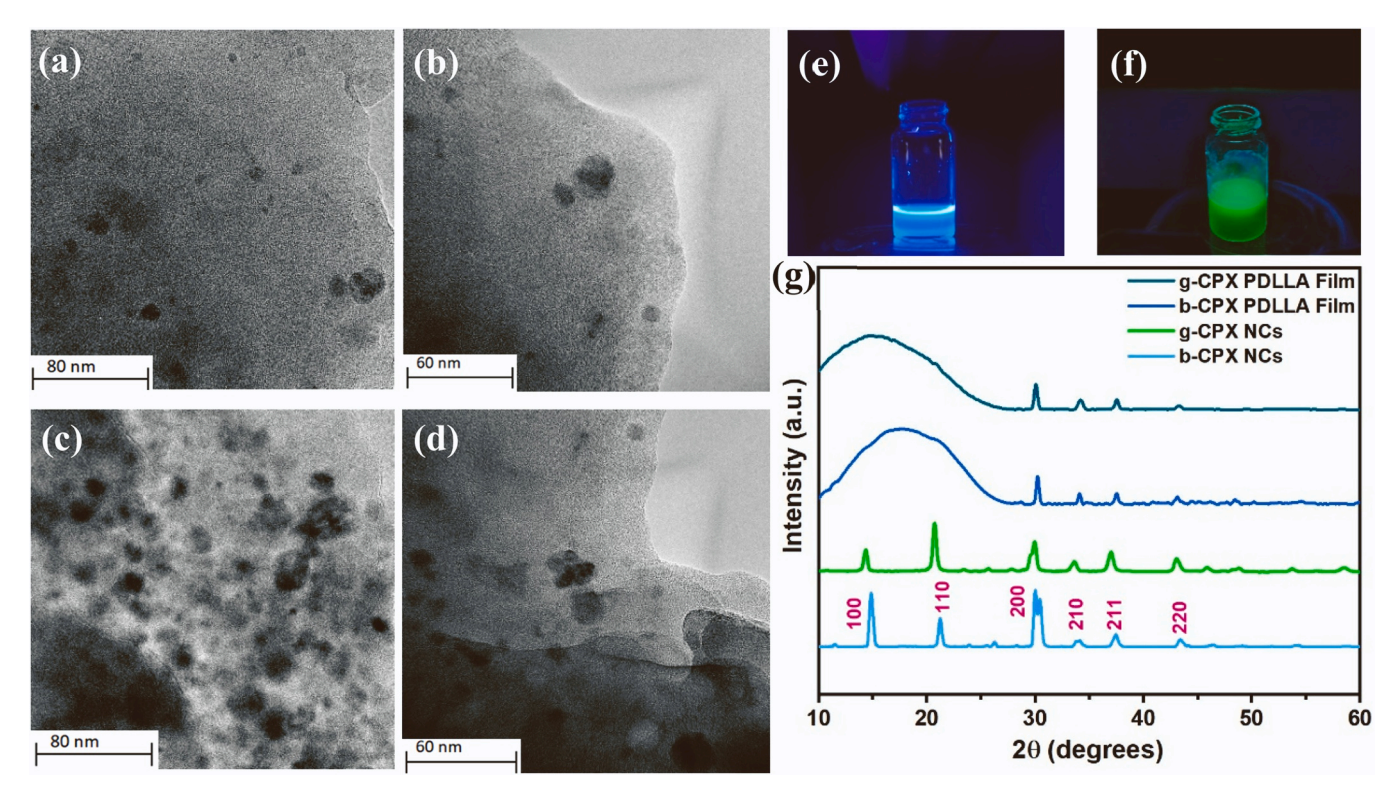


Fig. 2. TEM morphology of (a,b) b-CPX NCs and (c,d) g-CPX NCs. (e,f) Electronic images of photo luminous b-CPX and g-CPX NCs in Toluene solution under UV light at 364 nm wavelength excitation. (g) XRD pattern of b-CPX, g-CPX NCs, b-CPX PDLLA and g-CPX PDLLA film.

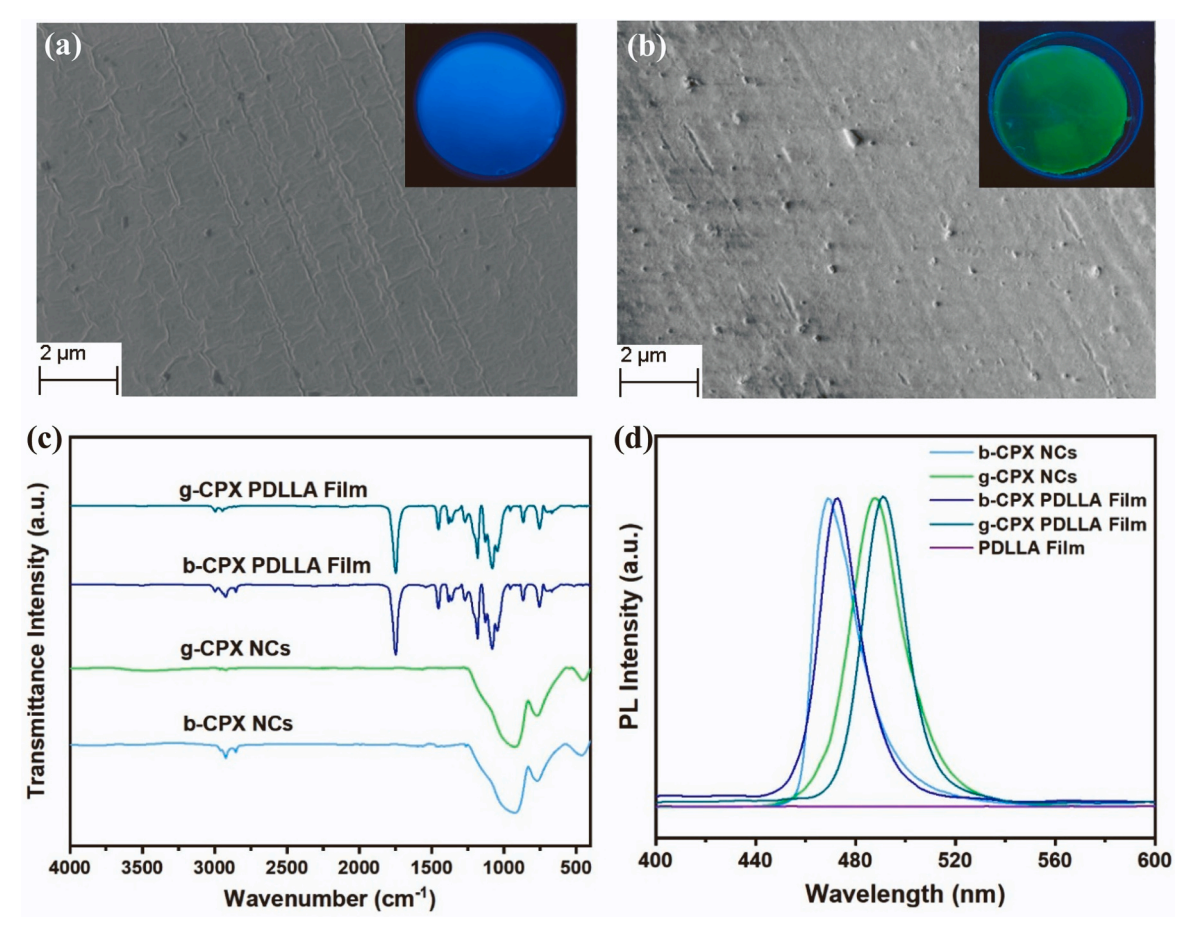


Fig. 3. (a,b) FESEM micrographs of b-CPX and g-CPX PDLLA films. FTIR (c) and PL emission (d) spectra of b-CPX and g-CPX NCs, b-CPX and g-CPX PDLLA films.

shifts slightly left for the g-CPX NCs which can be attributed to the thermal effect on the NCs and possible expansion of the unit cell and shifting of the peaks to a slightly lower angle (space groupPm3m, PDF#73-0692) [19]. Moreover, the PDLLA polymer matrix masked the lower angle peaks of the b-CPX and g-CPX NCs specially for $2\theta < 28^\circ$, although higher angle peaks of the NCs were still observable for the PDLLA encapsulated CsPbX $_3$ polymer composite films indicating that the intrinsic crystal structure of the NCs were still maintained in the CPX-PDLLA polymer films. The broader peaks in the range of 10° to 28° ascribed the PDLLA polymer.

The FESEM morphology of the b-CPX and g-CPX PDLLA films are illustrated in Fig. 3a and b. Dents on the surface of the films can be observed from these figures. This result can be attributed to air being accumulated and trapped at the time of pouring the perovskite polymer solution into the petri dish and air drying out when heated in the oven. It yielded traces on the surface, but no air bubbles were observed inside the film. The SEM images in Fig. 3a and b were utilized to further obtain the energy-dispersive X-ray spectroscopy (EDX) spectrum of the CsPbX₃-PDLLA films (Fig S1), C, O, and Cl were found occupied in the K shell and observed a voltage of 0.28, 0.525 and 2.625 KeV, respectively, whereas Cs and Br were occupied in the L shell and Pb in the M shell with an observed voltage of 4.3, 1.48 and 2.39 KeV, respectively. As shown in Fig. S1a and b, the atomic ratio of Cs, Pb, and (Cl+Br) is 0.82: 0.76: 2.42 (b-CPX PDLLA film) and 0.97: 0.9: 2.82 (g-CPX PDLLA film) which equals the CsPbX3 stoichiometric ratio [54,55]. Moreover, the Cl/Br ratio in the b-CPX PDLLA film (Fig S1a) is 1.94: 0.48, whereas in the g-CPX PDLLA film (Fig S1b) the ratio observed was 1.33: 1.52. This signifies the high concentration of Cl present compared to the Br (b-CPX PDLLA film) and vice versa. The variation in the Cl/Br ratio could be ascribed to the heat treatment at 150 °C for the g-CPX NCs [19].

The FTIR spectra of both b-CPX and g-CPX NCs and their associated CPX-PDLLA PENG films are shown in Fig. 3c. The weak broad IR peaks at approximately ~3400 cm⁻¹ for bare b-CPX and g-CPX NCs were attributed to -OH stretching of the carboxylic group of OLA [19,56]. The characteristic vibration at 2954 cm⁻¹ corresponded to the stretching of N-H of OA and the characteristic vibrations 2856 and 2350 cm⁻¹ corresponded to the O-C=O stretching and the asymmetric stretching of CH₃ [19,56,57]. The IR band around 1450 cm⁻¹ is characterized by -NH₂/-COO vibration arising from the amine/carboxylic acid group [19,58]. The -COO stretching at 1525 and 1553 cm⁻¹ conferred to the binding of Pb-oleate species [59]. The distinctive stretching at the low wavenumber region (750–900 cm⁻¹) is attributed to the Pb-X bonds present in bare b-CPX and g-CPX NCs while peaks at 908 cm⁻¹ is attributed to the C=C bending vibration [19,57]. The intensity of the peaks ranged from $2800 \text{ to } 3000 \text{ cm}^{-1}$ and reduced for the g-CPX NCs. This corresponding induced variation could be conferred due to the heat treatment at 150 °C for g-CPX NCs. However, interestingly all the NC bands are completely masked when encapsulated by the PDLLA polymer matrix (b-CPX and g-CPX PDLLA polymer film). PDLLA shows O-H stretching in the range of 3000–3600 cm⁻¹ in the IR band [60]. The characteristic sharp peaks at 2995, 2946, 1746 and 1080–1180 cm⁻¹ are due to the -CH3 asymmetric, -CH3 symmetric, C=O, C-O bonding stretching respectively of PDLLA polymer [61-63]. The peaks at 864 and 754 cm⁻¹ corresponded to the amorphous and crystalline phase of PDLLA [64]. The presence of weak peaks at 1380 cm⁻¹ (C–H symmetric bending vibration) [65] and 1125 cm⁻¹ (C-O-C stretching) [66] corrresponded to the α and γ phases contributing to low piezoelectric response. Moreover, the inclusion of CPX NCs improved crystallinity and the strong β phase dominance at 864 and 1210 cm⁻¹ absorption bands due to C-O-C stretching [52,65,66] brought by the interaction of CsPbX3 and the C-O-C dipoles enhanced overall polarization in the hybrid composite contributing to the increase of piezoelectric response, as similarly suggested by Mondal et al. for PVDF nanofiber with CsPbBr₃ and CsPbCl₃ [32,34].

The PL spectra of b-CPX & g-CPX NCs and their corresponding encapsulated b-CPX & g-CPX PDLLA films at $365\,\mathrm{nm}$ wavelength

excitation are shown in Fig. 3d. The PL spectra of b-CPX NCs depicted a blue luminescence band located approximately at 469 nm and PL spectra of g-CPX NCs depicted a green luminescence located approximately at 488 nm. These narrow PL emissions with a full width at half maximum (FWHM) of 20 nm (b-CPX NCs) and 24 nm (g-CPX NCs) is assigned to the CsPb(Cl/Br)₃ host involving band to band transition [26, 31].

Interestingly, these peaks further narrow down with a FWHMs of 19 nm and 20 nm for b-CPX PDLLA and g-CPX PDLLA films, respectively. This PL spectra of encapsulated films additionally shows a red shift to 473 nm for the b-CPX PDLLA film and 491 nm for the g-CPX PDLLA film [19,26]. This red shift in combination to narrowed FWHM's for NCs embedded films can be attributed to the loading of bigger NCs from the ensemble or a fractional size enhancement during the fabrication of the b-CPX and g-CPX PDLLA films [19,29]. Fig. 3d also shows the PDLLA film PL spectra resembling the background of the PL machine and confirms no observable luminescence from the PDLLA films. Interestingly, similar color tuning capabilities can also be observed in mechanically strong β -Ga₂O₃, β -(Ga_{0.955}Al_{0.045})₂O₃ and β -(Ga_{0.91}In_{0.09})₂O₃ solid films [67,68], however the mechanism for color tuning for these solid films is different in comparison to b-CPX and g-CPX nanocrytals embeded PDLLA films.

The fabricated PENG is shown in Fig. 4a and the working mechanism of the nanogenerator is illustrated in Fig. 4b. When the fabricated PENG is compressed, a piezoelectric field was generated along two opposite surfaces of the CPX-PDLLA film creating opposite poles [69,70]. As a result, induced electrostatic charges accumulated at the top and bottom surfaces of the CPX-PDLLA PENG yielding an electron flow through the connected external circuit [71,72]. During the release mode, the withdrawal of the piezo-potential led the induced charge to flow in the reverse (back) direction, and the combined press and release modes ultimately resulted in the alternation current signal [71,73]. Initially, the bare PDLLA piezoelectric film was tested to get electric performance as open circuit voltage (V_{oc}) and short circuit current (I_{sc}). To inspect the performance, we hand tapped the PENGs at 60 beats per minute (bpm) (1 Hz), 120 bpm (2 Hz), 180 bpm (3 Hz) and 240 bpm (4 Hz) load frequencies while keeping the range of motion at a distance of 8 cm (measure from the tip of the figure to the top surface of the PENG) [74]. The results in Fig. S2 shows that the individual PDLLA polymeric film resulted in obtaining a 4.4, 8.2, 14.3, 18.5 V maximum V_{oc} (Fig. S2a) and 3.45, 6.7, 10.2, 13.9 μ A maximum I_{sc} (Fig. S2b) at 60, 120, 180 and 240 bpm frequencies, respectively. This is due to the β phase presence and C=O dipole component generation [48,49,52] which were significantly lower in comparison to the b-CPX PDLLA and g-CPX PDLLA piezoelectric polymer composite presented in Fig. 4c-h. The recorded maximum V_{oc} for the b-CPX PDLLA PENG (Fig. 4c) at 60, 120, 180 and 240 bpm were 15.8, 25.2, 41.2, 55 V, respectively, whereas there is a further increase of the maximum V_{oc} observed for the g-CPX PDLLA PENG (Fig. 4f) at the same hand tapping motion (load frequencies) resulting in 31.5, 42.5, 65.4 and 92.8 V, respectively. Subsequently, a similar trend of I_{sc} enhancement was also noticed for the g-CPX PDLLA PENG in comparison to the b-CPX PDLLA PENG with short circuit current outputs of 13.8, $23.75, 37, 45.95 \mu A$ (b-CPX PDLLA PENG) and 23.4, 45.9, 48.2, 65.25 μ A (g-CPX PDLLA PENG), respectively. The enhancement of the electrical performance of the g-CPX PDLLA PENG can be attributed to the g-CPX NCs being agglomerated and clustered in the PDLLA matrix in comparison to the isolated b-CPX NCs in the PDLLA matrix and possible increment of electroactive β phase brought by the closely distributed g-CPX NCs in the PDLLA matrix [32-34]. Furthermore, average peak to peak voltages and current outputs were also measured and the results in Fig. 4e and h indicated that the highest average peak to peak voltage and current was 70.05 V and 60.98 μ A for the b-CPX PDLLA PENG at a 4 Hz load frequency, whilst for the g-CPX PDLLA PENG the measured outputs were 121.95 V and 88.38 μ A. The obtained results clearly implied that the g-CPX PDLLA PENG had a 74.13 % and 44.93 % increase of average peak to peak voltage and current in comparison to the b-CPX PDLLA

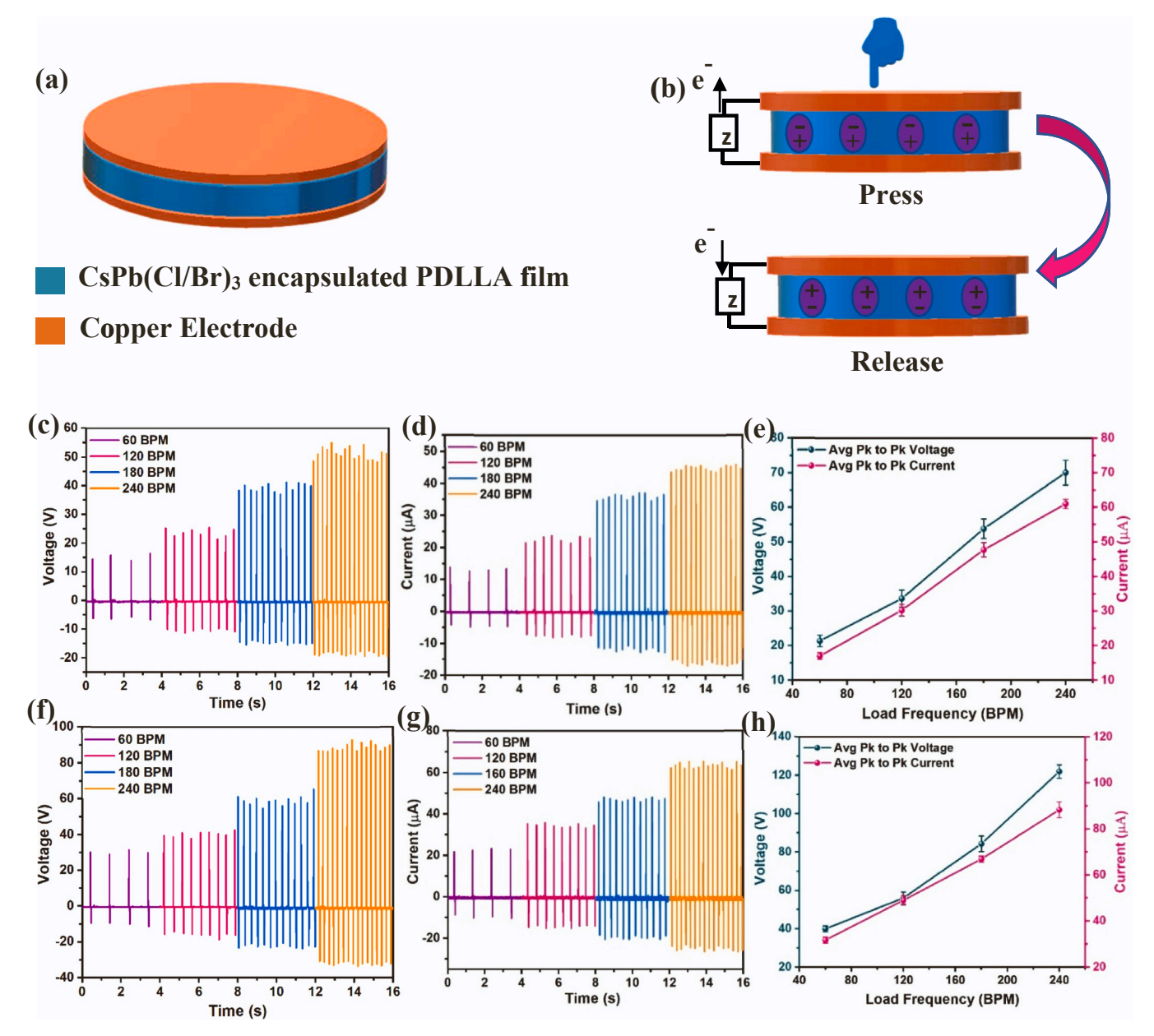


Fig. 4. (a) 3D schematic of CPX-PDLLA PENG. (b) Working mechanism (Press and release stage) of CPX-PDLLA PENG. Electrical performance of CPX-PDLLA PENG. (c,f) Open circuit voltage. (d,g) Short circuit current. (e,h) Maximum peak to peak voltage and current output of b-CPX PDLLA PENG and g-CPX PDLLA PENG, respectively, for 60, 120, 180, 240 bpm load frequency.

PENG reported above.

In addition, to further investigate the performance of the fabricated CsPbX₃-PDLLA PENG, we utilized a vertical constant force machine (schematic shown in Fig. 5e) where the load was varied from 10 to 30 psi with a load frequency of 65 bpm (Fig. 5a-d) [74]. The output electrical signal elucidated similar results in those observed in finger tapping but, the AC voltage and current peaks had higher uniformity. It can be highlighted that with the increase of the applied load, the impact force on the PENG surface also increased and the resultant AC V_{oc} observed was 3.72, 6.25, 10.22, 14.73, 20.8 V for b-CPX PDLLA PENG while the measured V_{oc} for the g-CPX PDLLA PENG was 8.4, 10, 22.8, 32.5, 45.2 V at 10, 15, 20, 25, and 35 psi, respectively (Fig. 5a and c). In addition, in Fig. 5b and d, the output I_{sc} also increased linearly and yielded 1.33, $1.94, 3.22, 4.75, 6.2 \mu A$ (b-CPX PDLLA PENG) and 2.7, 4.16, 7.96, 10.4,13.4 μ A (g-CPX PDLLA PENG) at 10, 15, 20, 25, and 30 psi, respectively. However, compared to the finger tapped electrical output, the V_{oc} and I_{sc} was significantly lower since the diameter of the circular piston of the force machine was 2.54 cm with an active contact area of 5.07 cm² while the effective contact area of the PENG films was 31.67 cm² indicating that the piston couldn't utilize the whole active.

area of the PENG [74,75]. Fig. 6c demonstrates that the full-wave bridge rectifier circuit converts the AC voltage signal of the PENG into direct current (DC) signal. The full wave rectification of the b-CPX and g-CPX PDLLA PENGs demonstrated in Fig. 6a and b that the maximum DC output was 26.1 and 35.2 V at a 180-bpm load frequency. The charging prospect of fabricated PENGs was also investigated with different capacitors and represents future applications in charging small electronic devices. The capacitance tests were performed with 1.0, 3.3, 4.7 and 10 μ F capacitors (Fig. 6f) for 30 s at a 240-hand tapping load frequency and the measured outputs, in Fig. 6d and e, exhibited that as the capacitance increased, the rate of charging decreased. The maximum charging output obtained for the b-CPX PDLLA PENG at 30 s was 2.68, 1.42, 1.16, 0.56 V whereas the measured maximum capacitance output for the g-CPX PDLLA PENG was 4.72, 3.18, 2.75, 1.79 V at 1.0, 3.3, 4.7

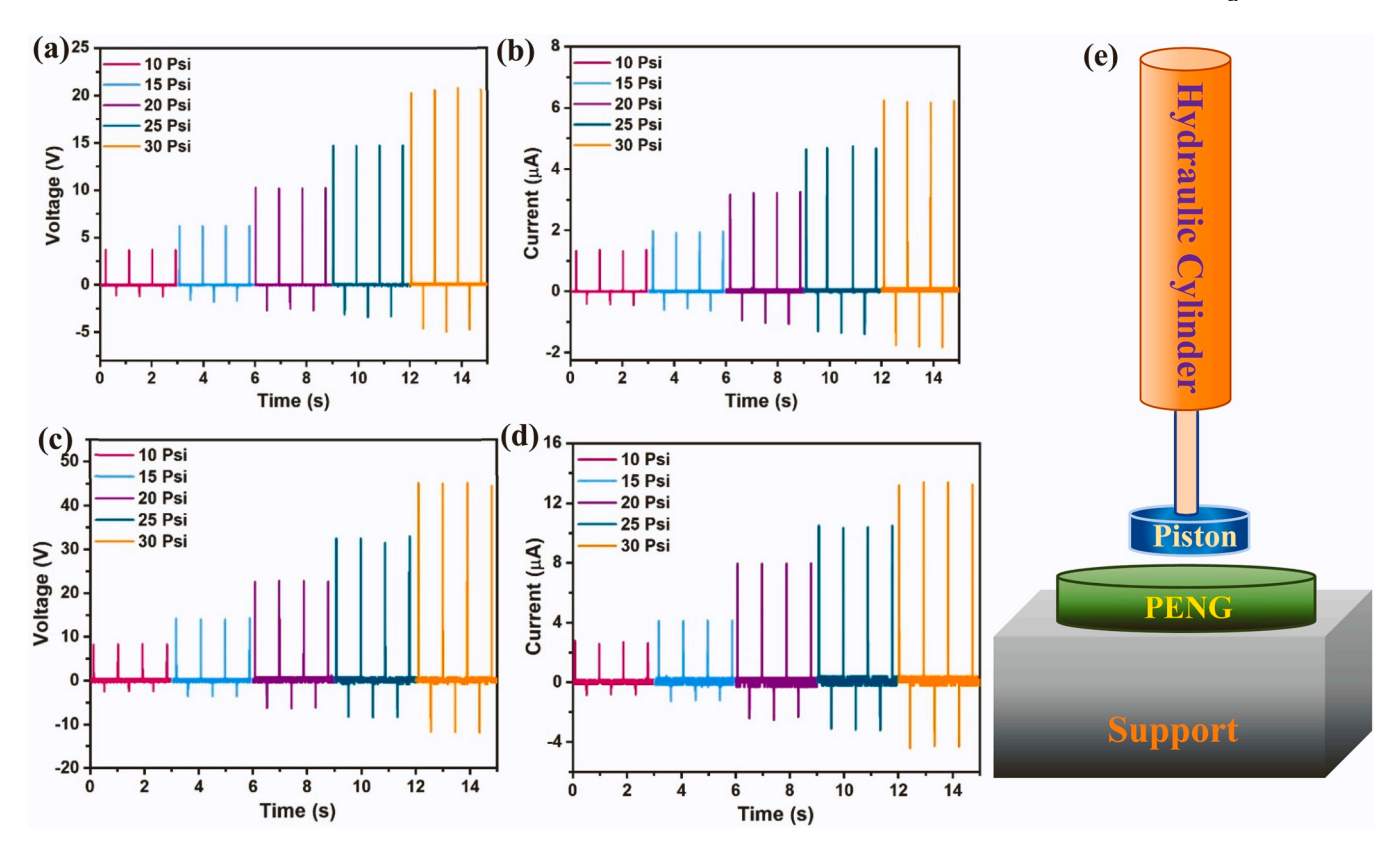


Fig. 5. Electrical performance of CPX-PDLLA PENG. (a,c) Open circuit voltage, (b,d) Short circuit current output and (e) Experimental set up for fixed pressure test of b-CPX PDLLA PENG and g-CPX PDLLA PENG for different pressure at 65 bpm load frequency.

and 10 μ F capacitance, respectively.

Furthermore, the PENGs were further tested in connection with external load resistances in series with a full bridge rectifier as shown in Fig. 6i. The resistive load varied from 0.5 M Ω to 15 M Ω at a 240 bpm (4 Hz) load frequency and the results in Fig. 6g and h revealed that the average voltage output increased while average current output declined with the increasing load resistance showing an opposing trend contrary to voltage output in accordance with Ohm's law [74]. In addition, the PENG will deliver maximum power when the external resistance (optimum load) will be equivalent to internal resistance of the device according to the maximum power theory [72]. As a result, the power output $(P = V^2/R)$ gradually escalated as a sharp increase of the output occurring from a 1.36–4.08 $M\Omega$ resistive load for both b-CPX and g-CPX PDLLA PENGs (Fig. 6g and According to the size of each PENG devices (31.67 cm^2) , the instantaneous power density obtained was ~10.67 μ W/cm² (b-CPX PDLLA PENG) and ~25.17 μ W/cm² (g-CPX PDLLA PENG). Additionally, the capability and feasibility of our fabricated PENGs were attached to a series of commercial LEDs connected with a full-wave bridge rectifier and a 0.1 μ F capacitor and interestingly the b-CPX and g-CPX PDLLA PENG was able to light up 20 and 50 commercial LEDs (1.5 V each), respectively (Video 1 & 2 in supplementary information). This demonstrates the prospective aspects of our flexible CsPbX₃ perovskite encapsulated PDLLA PENGs in flexible and stretchable electronic applications [5,76].

Supplementary material related to this article can be found online at doi:10.1016/j.nanoen.2022.107674.

4. Conclusion

In summary, we have synthesized color tuned (blue to green) photoluminescent all inorganic CPX NCs and further integrated a PDLLA polymer matrix to fabricate luminous CPX-PDLLA PENGs. Fine color tunability was achieved by a heat treatment process at 150 °C which

resulted in a possibility of a size increase and agglomeration of NCs in the case of g-CPX NCs in comparison to the monodispersed b-CPX NCs. PL emission spectra revealed that the encapsulation of the CsPbX3 NCs influenced the peaks to red shift from 469 nm (b-CPX NCs) to 473 nm (b-CPX PDLLA PENG) and 488 (g-CPX NCs) nm to 491 nm (g-CPX PDLLA PENG). The hand tapping PENG tests exhibited that with the increase of the load frequency (60-240 bpm), piezoelectric response (both open circuit voltage and short circuit current) increased gradually. The maximum V_{oc} and I_{sc} reported at 240 bpm (4 Hz frequency) for the g-CPX PDLLA PENG was 92.8 V and 65.25 μ A, respectively, which exhibited a 68.72 % and 35.47 % increment in comparison to the b-CPX PDLLA PENG. This can be attributed to the agglomerated polarizing effect in the case of the g-CPX NCs in comparison to the individual segregated poling effect in the b-CPX NCs. The high output of both PENG $\,$ devices can be accredited to the β phase presence and C=O dipole components resulted by the sharing effect of hand tapping motion. In addition, the improvement of electroactive β phase owing to the interaction of CsPbX3 and the C-O-C dipoles in PDLLA polymer matrix resulted in a supplementary piezoelectric effect. The constant pressure test conducted upon both PENG devices confirmed the uniform signal output was more random while hand tapping. Moreover, the capacitor tests highlighted that within just 30 s of hand tapping at a 4 Hz load frequency can charge up to a maximum voltage of 2.68 V (b-CPX PDLLA PENG) and 4.72 V (g-CPX PDLLA PENG) representing a high charging capability of the devices. Moreover, power versus variable resistance load was carried out from $0.5\,M\Omega$ to $15\,M\Omega$ and the highest power density achieved was $\sim 10.67 \ \mu \text{Wcm}^{-2}$ and $\sim 25.17 \ \mu \text{Wcm}^{-2}$ for the b-CPX and g-CPX PDLLA PENGs, at a 4.08 M Ω load resistance, respectively. The PENGs were able to light up 20 (b-CPX PDLLA PENG) and 50 commercial LEDs (g-CPX PDLLA PENG) which elucidates the promising nature of our fabricated self-charging flexible electronic device. Future studies include the synthesizing of the CPX NCs exhibiting an orange to red color tunability from the same precursor solution at ambient

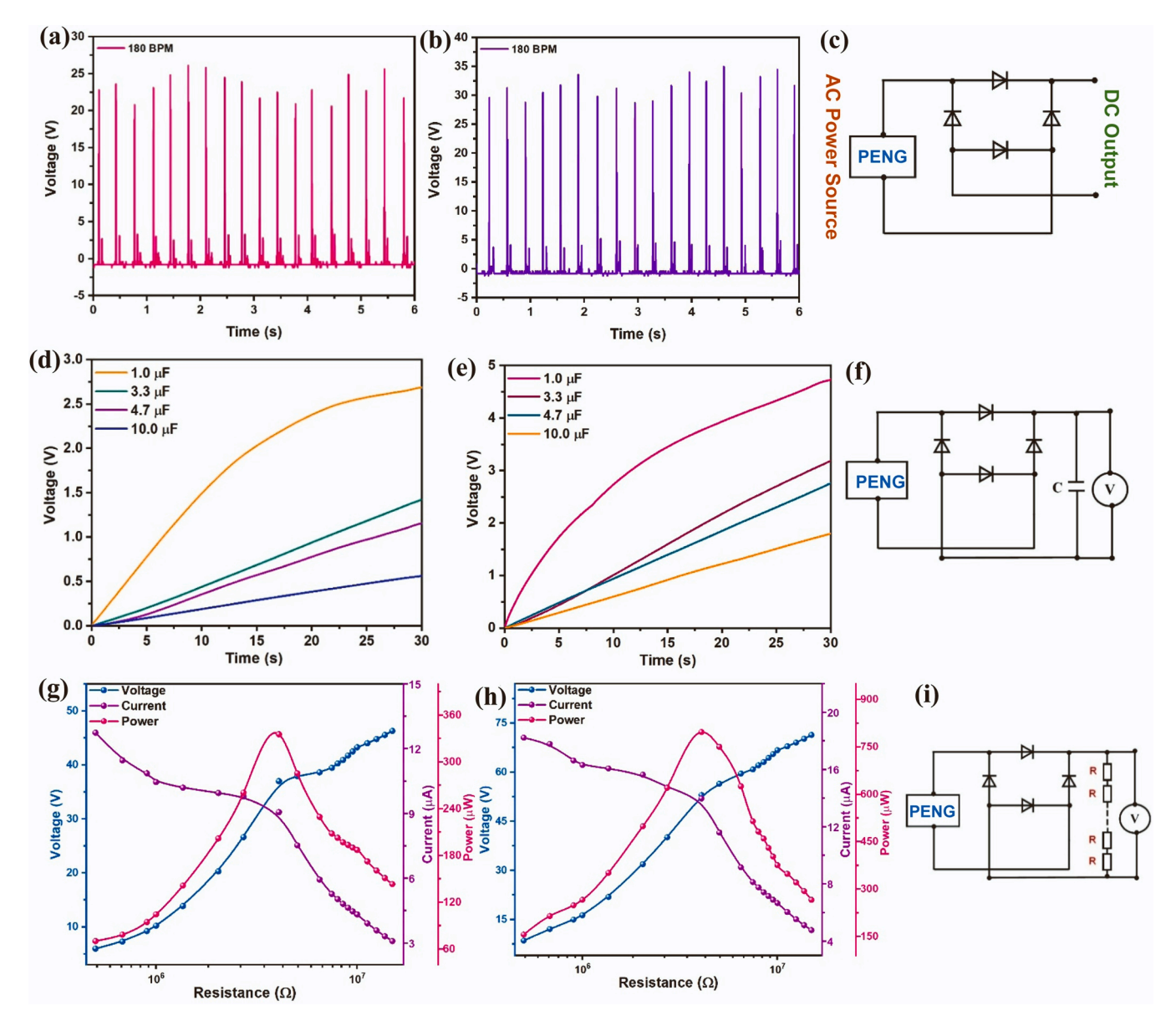


Fig. 6. Electrical performance of CPX-PDLLA PENG. (a,b) Rectified DC voltage output of b-CPX and g-CPX PDLLA PENG at 65 BPM load frequency and (c) Full bridge rectifier circuit. (d,e) Charging ability with different capacitors of b-CPX and g-CPX PDLLA PENG and (f) Capacitor test circuit. (g,h) Average voltage, current and power output of b-CPX and g-CPX PDLLA PENG with variable external resistance and (i) Resistance test circuit.

conditions and creating Pb free perovskite NCs for piezoelectric and triboelectric energy harvesting and sensor applications.

CRediT authorship contribution statement

Sk Shamim Hasan Abir: Conceptualization, Visualization, Methodology, Validation, Investigation, Data curation, Formal analysis. Julio E. Trevino, Bhupendra B. Srivastava, Muhtasim Ul Karim Sadafa, Julia I. Salasa: Asistance with characterization. Karen Lozano and Mohammed Jasim Uddin: Concept, Idea, Funding and Supervision.

Declaration of Competing Interest

The authors declare that they have no known competing financial interests or personal relationships that could have appeared to influence the work reported in this paper.

Data availability

Data will be made available on request.

Acknowledgements

The authors gratefully acknowledge the support received by US National Science Foundation (NSF) award under grant No. DMR-2122178 UTRGV-UMN Partnership to Strengthen the PREM Pathway. The authors would like to show gratitude to Dr. Ana Stevanovic (Kleberg Advanced Microscopy Center, University of Texas at San Antonio) for helping with TEM imaging of CsPbX₃ NCs. MJU acknowledges the support from Welch Foundation Grant (2022-2025; BX 0048).

Appendix A. Supporting information

Supplementary data associated with this article can be found in the online version at doi:10.1016/j.nanoen.2022.107674.

References

- [1] S. Poopak, A.R. Reza, H. Ujita, F. Duan, D. Vatansever, E. Siores, in: Bharat Raj Singh, (Ed.), Global Warming – Impacts and Future, 2017.
- [2] D. Lopez, A.R. Chowdhury, A.M. Abdullah, M.U.K. Sadaf, I. Martinez, B. D. Choudhury, S. Danti, C.J. Ellison, K. Lozano, M.J. Uddin, Polymer based triboelectric nanogenerator for cost-effective green energy generation and implementation of surface-charge engineering, Energy Technol. (2021), 2001088, https://doi.org/10.1002/ente.202001088.
- [3] D. Zamora, A.M. Abdullah, A. Flores, H. Majumder, M.U.K. Sadaf, B. Azimi, S. Danti, M.J. Uddin, Flexible bielectrode based highly sensitive triboelectric motion sensor: a sustainable and smart electronic material, Energy Technol. 2100662 (2022) 1–8, https://doi.org/10.1002/ente.202100662.
- [4] A. Ballato, Piezoelectricity: history and new thrusts, in: Proceedings of the IEEE Ultrason. Symp. 1 (1996) 575–583. (https://doi.org/10.1109/ultsym.1996.584046
- [5] A.M. Abdullah, M.U.K. Sadaf, F. Tasnim, H. Vasquez, K. Lozano, M.J. Uddin, KNN based piezo-triboelectric lead-free hybrid energy films, Nano Energy 86 (2021), 106133. https://doi.org/10.1016/j.nanoen.2021.106133.
- [6] D. Hu, M. Yao, Y. Fan, C. Ma, M. Fan, M. Liu, Strategies to achieve high performance piezoelectric nanogenerators, Nano Energy 55 (2019) 288–304, https://doi.org/10.1016/j.nanoen.2018.10.053.
- [7] F. Rubaiya, S. Mohan, B.B. Srivastava, H. Vasquez, K. Lozano, Piezoelectric properties of PVDF-Zn2GeO4 fine fiber mats, Energies 14 (2021), https://doi.org/ 10.3390/en14185936
- [8] J.E. Trevino, S. Mohan, A.E. Salinas, E. Cueva, K. Lozano, Piezoelectric properties of PVDF-conjugated polymer nanofibers, J. Appl. Polym. Sci. (2021), https://doi. org/10.1002/app.50665
- [9] S. Park, Y. Kim, H. Jung, J.Y. Park, N. Lee, Y. Seo, Energy harvesting efficiency of piezoelectric polymer film with graphene and metal electrodes, Sci. Rep. 7 (2017) 1–8, https://doi.org/10.1038/s41598-017-17791-3.
- [10] Z. Wang, H. Kurita, H. Nagaoka, F. Narita, Potassium sodium niobate lead-free piezoelectric nanocomposite generators based on carbon-fiber-reinforced polymer electrodes for energy-harvesting structures, Compos. Sci. Technol. 199 (2020), 108331, https://doi.org/10.1016/j.compscitech.2020.108331.
- [11] M.A. Johar, M.A. Hassan, A. Waseem, J.S. Ha, J.K. Lee, S.W. Ryu, Stable and high piezoelectric output of GaN nanowire-based lead-free piezoelectric nanogenerator by suppression of internal screening, Nanomaterials 8 (2018), https://doi.org/ 10.3390/nano8060437
- [12] W. Qin, T. Li, Y. Li, J. Qiu, X. Ma, X. Chen, X. Hu, W. Zhang, A high power ZnO thin film piezoelectric generator, Appl. Surf. Sci. 364 (2016) 670–675, https://doi.org/ 10.1016/j.apsusc.2015.12.178.
- [13] H. Liu, X. Lin, S. Zhang, Y. Huan, S. Huang, X. Cheng, Enhanced performance of piezoelectric composite nanogenerator based on gradient porous PZT ceramic structure for energy harvesting, J. Mater. Chem. A 8 (2020) 19631–19640, https:// doi.org/10.1039/d0ta03054f.
- [14] K.B. Kim, J.Y. Cho, J. Hamid, J.H. Ahn, S. Do Hong, S.B. Woo, T.H. Sung, Optimized composite piezoelectric energy harvesting floor tile for smart home energy management, Energy Convers. Manag. 171 (2018) 31–37, https://doi.org/ 10.1016/j.enconman.2018.05.031.
- [15] S. Ippili, V. Jella, A.M. Thomas, S.-G. Yoon, The recent progress on halide perovskite-based self-powered sensors enabled by piezoelectric and triboelectric effects, Nanoenergy Adv. 1 (2021) 3–31, https://doi.org/10.3390/ nanoenergyadv1010002.
- [16] Y.J. Kim, T. Van Dang, H.J. Choi, B.J. Park, J.H. Eom, H.A. Song, D. Seol, Y. Kim, S. H. Shin, J. Nah, S.G. Yoon, Piezoelectric properties of CH3NH3PbI3 perovskite thin films and their applications in piezoelectric generators, J. Mater. Chem. A 4 (2016) 756–763, https://doi.org/10.1039/c5ta09662f.
- [17] R. Ding, H. Liu, X. Zhang, J. Xiao, R. Kishor, H. Sun, B. Zhu, G. Chen, F. Gao, X. Feng, J. Chen, X. Chen, X. Sun, Y. Zheng, Flexible piezoelectric nanocomposite generators based on formamidinium lead halide perovskite nanoparticles, Adv. Funct. Mater. 26 (2016) 7708–7716, https://doi.org/10.1002/adfm.201602634.
- [18] J. Hao, W. Li, J. Zhai, H. Chen, Progress in high-strain perovskite piezoelectric ceramics, Mater. Sci. Eng. R Rep. 135 (2019) 1–57, https://doi.org/10.1016/j. progr 2018 08 001
- [19] S.S.H. Abir, S.K. Gupta, A. Ibrahim, B.B. Srivastava, K. Lozano, Tunable CsPb(Br/Cl) 3 perovskite nanocrystals and further advancement in designing light emitting fiber membranes, Mater. Adv. 2 (2021) 2700–2710, https://doi.org/10.1039/dlma00183c.
- [20] J. Song, J. Li, X. Li, L. Xu, Y. Dong, H. Zeng, Quantum dot light-emitting diodes based on inorganic perovskite cesium lead halides (CsPbX3, Adv. Mater. 27 (2015) 7162–7167, https://doi.org/10.1002/adma.201502567.
- [21] J. Du, X. Yang, J. Duan, Y. Wang, Q. Tang, Tailoring all-inorganic cesium lead halide perovskites for robust triboelectric nanogenerators, Nano Energy 70 (2020), 104514, https://doi.org/10.1016/j.nanoen.2020.104514.
- [22] Z.L. Wang, J. Song, Piezoelectric nanogenerators based on zinc oxide nanowire arrays, Science 312 (2006) 242–246, https://doi.org/10.1126/science.1124005.
- [23] R. Ding, X. Zhang, G. Chen, H. Wang, R. Kishor, J. Xiao, F. Gao, K. Zeng, X. Chen, X. W. Sun, Y. Zheng, High-performance piezoelectric nanogenerators composed of formamidinium lead halide perovskite nanoparticles and poly(vinylidene fluoride, Nano Energy 37 (2017) 126–135, https://doi.org/10.1016/j.nanoen.2017.05.010.
- [24] H. Chen, F. Zhou, Z. Jin, Interface engineering, the trump-card for CsPbX3 (X⁻I, Br) perovskite solar cells development, Nano Energy 79 (2021), 105490, https://doi.org/10.1016/j.nanoen.2020.105490.

- [25] M.J.H. Tan, Y. Chan, Pulsed laser photopatterning of cesium lead halide perovskite structures as robust solution-processed optical gain media, Adv. Mater. Technol. 5 (2020) 1–8, https://doi.org/10.1002/admt.202000104.
- [26] M. Yang, J. Yu, S. Jiang, C. Zhang, Q. Sun, M. Wang, H. Zhou, C. Li, B. Man, F. Lei, High stability luminophores: fluorescent CsPbX 3 (X = Cl, Br and I) nanofiber prepared by one-step electrospinning method, Opt. Express 26 (2018) 20649, https://doi.org/10.1364/oe.26.020649.
- [27] G. Gao, Q. Xi, H. Zhou, Y. Zhao, C. Wu, L. Wang, P. Guo, J. Xu, Novel inorganic perovskite quantum dots for photocatalysis, Nanoscale 9 (2017) 12032–12038, https://doi.org/10.1039/c7nr04421f.
- [28] X. Li, D. Yu, J. Chen, Y. Wang, F. Cao, Y. Wei, Y. Wu, L. Wang, Y. Zhu, Z. Sun, J. Ji, Y. Shen, H. Sun, H. Zeng, Constructing fast carrier tracks into flexible perovskite photodetectors to greatly improve responsivity, ACS Nano 11 (2017) 2015–2023, https://doi.org/10.1021/acsnano.6b08194.
- [29] L. Chen, Y. Chuang, W.D. Yang, K.C. Tsai, C.W. Chen, C. Di Dong, All-inorganic perovskite CsPbX3 electrospun nanofibers with color-tunable photoluminescence and high performance optoelectronic applications, J. Alloy. Compd. 856 (2021), 157426, https://doi.org/10.1016/j.jallcom.2020.157426.
- [30] L. Protesescu, S. Yakunin, M.I. Bodnarchuk, F. Krieg, R. Caputo, C.H. Hendon, R. X. Yang, A. Walsh, M.V. Kovalenko, Nanocrystals of cesium lead halide perovskites (CsPbX3, X = Cl, Br, and I): novel optoelectronic materials showing bright emission with wide color gamut, Nano Lett. 15 (2015) 3692–3696, https://doi.org/10.1021/nl5048779.
- [31] Y. Huang, T. Wang, J. Zheng, F. Li, W. Lan, F. Zheng, S. Li, Multiwalled carbon nanotubes/CsPbX3@polyacrylonitrile core/shell nanofibers with ultrahigh water, thermal, and ultraviolet stability, Macromol. Mater. Eng. 306 (2021) 1–8, https://doi.org/10.1002/mame.202100200.
- [32] S. Mondal, T. Paul, S. Maiti, B.K. Das, K.K. Chattopadhyay, Human motion interactive mechanical energy harvester based on all inorganic perovskite-PVDF, Nano Energy 74 (2020), 104870, https://doi.org/10.1016/j.nanoen.2020.104870.
- [33] H. Chen, L. Zhou, Z. Fang, S. Wang, T. Yang, L. Zhu, X. Hou, H. Wang, Z.L. Wang, Piezoelectric nanogenerator based on in situ growth all-inorganic CsPbBr3 perovskite nanocrystals in PVDF fibers with long-term stability, Adv. Funct. Mater. 31 (2021) 1–12, https://doi.org/10.1002/adfm.202011073.
- [34] S. Mondal, S. Maiti, T. Paul, A. Sahoo, S. Bhattacharjee, N.S. Das, K. K. Chattopadhyay, All-inorganic halide perovskite tuned robust mechanical-energy harvester: self driven posture monitor and power source for portable electronics, Appl. Mater. Today 26 (2022), 101385, https://doi.org/10.1016/j.apmt.2022.101385.
- [35] P. Vashishtha, J.E. Halpert, Field-driven ion migration and color instability in Redemitting mixed halide perovskite nanocrystal light-emitting diodes, Chem. Mater. 29 (2017) 5965–5973, https://doi.org/10.1021/acs.chemmater.7b01609.
- [36] X. Zhang, X. Bai, H. Wu, X. Zhang, C. Sun, Y. Zhang, W. Zhang, W. Zheng, W.W. Yu, A.L. Rogach, Water-assisted size and shape control of CsPbBr3 perovskite nanocrystals, Angew. Chem. Int. Ed. 57 (2018) 3337–3342, https://doi.org/ 10.1002/anje.201710869.
- [37] Y. Tong, E. Bladt, M.F. Aygüler, A. Manzi, K.Z. Milowska, V.A. Hintermayr, P. Docampo, S. Bals, A.S. Urban, L. Polavarapu, J. Feldmann, Highly Luminescent cesium lead halide perovskite nanocrystals with tunable composition and thickness by ultrasonication, Angew. Chem. Int. Ed. 55 (2016) 13887–13892, https://doi. org/10.1002/anie.201605909.
- [38] J. Chen, Y. Fu, L. Samad, L. Dang, Y. Zhao, S. Shen, L. Guo, S. Jin, Vapor-phase epitaxial growth of aligned nanowire networks of cesium lead halide perovskites (CsPbX3, X = Cl, Br, I), Nano Lett. 17 (2020) 460–466, https://doi.org/10.1021/acs.nanolett.6b04450.
- [39] L. Protesescu, S. Yakunin, O. Nazarenko, D.N. Dirin, M.V. Kovalenko, Low-cost synthesis of highly luminescent colloidal lead halide perovskite nanocrystals by wet ball milling, ACS Appl. Nano Mater. 1 (2018) 1300–1308, https://doi.org/ 10.1021/acsanm.8b00038.
- [40] Q. Pan, H. Hu, Y. Zou, M. Chen, L. Wu, D. Yang, X. Yuan, J. Fan, B. Sun, Q. Zhang, Microwave-assisted synthesis of high-quality "all-inorganic" CsPbX3 (X = Cl, Br, I) perovskite nanocrystals and their application in light emitting diodes, J. Mater. Chem. C 5 (2017) 10947–10954, https://doi.org/10.1039/c7tc03774k.
- [41] P.V. Kamat, N. Pradhan, K. Schanze, P.S. Weiss, J. Buriak, P. Stang, T.W. Odom, G. Hartland, Challenges and opportunities in designing perovskite nanocrystal heterostructures, ACS Energy Lett. 5 (2020) 2253–2255, https://doi.org/10.1021/ acsenergylett.0c01216.
- [42] X. Li, D. Yu, F. Cao, Y. Gu, Y. Wei, Y. Wu, J. Song, H. Zeng, Healing all-inorganic perovskite films via recyclable dissolution–recyrstallization for compact and smooth carrier channels of optoelectronic devices with high stability, Adv. Funct. Mater. 26 (2016) 5903–5912, https://doi.org/10.1002/adfm.201601571.
- [43] F. Zhang, S. Huang, P. Wang, X. Chen, S. Zhao, Y. Dong, H. Zhong, Colloidal synthesis of air-stable CH3NH3PbI3 quantum dots by gaining chemical insight into the solvent effects, Chem. Mater. 29 (2017) 3793–3799, https://doi.org/10.1021/ acs.chemmater.7b01100.
- [44] S. Bose, J.R. Summers, B.B. Srivastava, V. Padilla-Gainza, M. Peredo, C.M. Trevino De Leo, B. Hoke, S.K. Gupta, K. Lozano, Efficient near infrared to visible light upconversion from Er/Yb codoped PVDF fibrous mats synthesized using a direct polymer doping technique, Opt. Mater. 123 (2022), https://doi.org/10.1016/j. optmat.2021.111866.
- [45] Z. Li, L. Kong, S. Huang, L. Li, Highly luminescent and ultrastable CsPbBr3 perovskite quantum dots incorporated into a silica/alumina monolith, Angew. Chem. Int. Ed. 56 (2017) 8134–8138, https://doi.org/10.1002/anie.20170326
- [46] A. Loiudice, S. Saris, E. Oveisi, D.T.L. Alexander, R. Buonsanti, CsPbBr3 QD/AlOx inorganic nanocomposites with exceptional stability in water, light, and heat,

Angew. Chem. Int. Ed. 56 (2017) 10696–10701, https://doi.org/10.1002/

S.S.H. Abir et al.

- [47] T. Tábi, T. Ageyeva, J.G. Kovács, Improving the ductility and heat deflection temperature of injection molded Poly(lactic acid) products: a comprehensive review, Polym. Test. 101 (2021), https://doi.org/10.1016/j. polymertesting.2021.107282.
- [48] S. Gong, B. Zhang, J. Zhang, Z.L. Wang, K. Ren, Biocompatible poly(lactic acid)-based hybrid piezoelectric and electret nanogenerator for electronic skin applications, Adv. Funct. Mater. 30 (2020), https://doi.org/10.1002/adfm.201908724.
- [49] C. Zhao, J. Zhang, Z.L. Wang, K. Ren, A poly(l-lactic acid) polymer-based thermally stable cantilever for vibration energy harvesting applications, Adv. Sustain. Syst. 1 (2017), https://doi.org/10.1002/adsu.201700068.
- [50] G. Zhao, B. Huang, J. Zhang, A. Wang, K. Ren, Z.L. Wang, Electrospun poly(l-lactic acid) nanofibers for nanogenerator and diagnostic sensor applications, Macromol. Mater. Eng. 302 (2017), https://doi.org/10.1002/mame.201600476.
- [51] S.J. Lee, A.P. Arun, K.J. Kim, Piezoelectric properties of electrospun poly(l-lactic acid) nanofiber web, Mater. Lett. 148 (2015) 58–62, https://doi.org/10.1016/j. matlet 2015 02 038
- [52] K. Oumghar, N. Chakhchaoui, R. Farhan, A. Eddiai, M. Meddad, O. Cherkaoui, M. Mazroui, L. Van Langenhove, Piezoelectric β-polymorph enhancement in graphene oxide -PLA nanocomposite films, IOP Conf. Ser. Mater. Sci. Eng. 948 (2020). https://doi.org/10.1088/1757-899X/948/1/012024.
- [53] C. Wang, H. Lin, Z. Zhang, Z. Qiu, H. Yang, Y. Cheng, J. Xu, X. Xiang, L. Zhang, Y. Wang, X-ray excited CsPb(Cl,Br)3 perovskite quantum dots-glass composite with long-lifetime, J. Eur. Ceram. Soc. 40 (2020) 2234–2238, https://doi.org/10.1016/ i.jeurceramsoc.2020.01.016.
- [54] T. Paul, B.K. Chatterjee, S. Maiti, S. Sarkar, N. Besra, B.K. Das, K.J. Panigrahi, S. Thakur, U.K. Ghorai, K.K. Chattopadhyay, Tunable cathodoluminescence over the entire visible window from all-inorganic perovskite CsPbX3 1D architecture, J. Mater. Chem. C 6 (2018) 3322–3333, https://doi.org/10.1039/c7tc05703b.
- [55] Z. Hu, Z. Liu, Y. Bian, D. Liu, X. Tang, W. Hu, Z. Zang, M. Zhou, L. Sun, J. Tang, Y. Li, J. Du, Y. Leng, Robust cesium lead halide perovskite microcubes for frequency upconversion lasing, Adv. Opt. Mater. 5 (2017) 1–8, https://doi.org/10.1002/adom.201700419.
- [56] Z. Bao, W. Wang, H.Y. Tsai, H.C. Wang, S. Chen, R.S. Liu, Photo-/electro-luminescence enhancement of CsPbX3 (X = Cl, Br, or I) perovskite quantum dots via thiocyanate surface modification, J. Mater. Chem. C 8 (2020) 1065–1071, https://doi.org/10.1039/c9tc05448k.
- [57] Y. Chang, Y.J. Yoon, G. Li, E. Xu, S. Yu, C.H. Lu, Z. Wang, Y. He, C.H. Lin, B. K. Wagner, V.V. Tsukruk, Z. Kang, N. Thadhani, Y. Jiang, Z. Lin, All-Inorganic perovskite nanocrystals with a stellar set of stabilities and their use in white lightemitting diodes, ACS Appl. Mater. Interfaces 10 (2018) 37267–37276, https://doi.org/10.1021/acsami.8b13553.
- [58] H.C. Yoon, S. Lee, J.K. Song, H. Yang, Y.R. Do, Efficient and stable CsPbBr3 quantum-dot powders passivated and encapsulated with a mixed silicon nitride and silicon oxide inorganic polymer matrix, ACS Appl. Mater. Interfaces 10 (2018) 11756–11767. https://doi.org/10.1021/acsami.8b01014.
- [59] E. Yassitepe, Z. Yang, O. Voznyy, Y. Kim, G. Walters, J.A. Castañeda, P. Kanjanaboos, M. Yuan, X. Gong, F. Fan, J. Pan, S. Hoogland, R. Comin, O. M. Bakr, L.A. Padilha, A.F. Nogueira, E.H. Sargent, Amine-free synthesis of cesium lead halide perovskite quantum dots for efficient light-emitting diodes, Adv. Funct. Mater. 26 (2016) 8757–8763, https://doi.org/10.1002/adfm.201604580.
- [60] J.P. Mofokeng, A.S. Luyt, T. Tábi, J. Kovács, Comparison of injection moulded, natural fibre-reinforced composites with PP and PLA as matrices, J. Thermoplast. Compos. Mater. 25 (2012) 927–948, https://doi.org/10.1177/ 0892705711423291.
- [61] J. Du, Y. Wang, X. Xie, M. Xu, Y. Song, Styrene-assisted maleic anhydride grafted poly(lactic acid) as an effective compatibilizer for wood flour/poly(lactic acid) biocomposites, Polymers 9 (2017), https://doi.org/10.3390/polym9110623.
- [62] V.S. Giita Silverajah, N.A. Ibrahim, N. Zainuddin, W.M.Z. Wan Yunus, H.A. Hassan, Mechanical, thermal and morphological properties of poly(lactic acid)/epoxidized palm olein blend, Molecules 17 (2012) 11729–11747, https://doi.org/10.3390/ prolegiles/17/101779
- [63] B.W. Chieng, N.A. Ibrahim, W.M.Z.W. Yunus, M.Z. Hussein, Poly(lactic acid)/poly (ethylene glycol) polymer nanocomposites: effects of graphene nanoplatelets, Polymers 6 (2014) 93–104, https://doi.org/10.3390/polym6010093.
- [64] E.E. Popa, M. Rapa, O. Popa, G. Mustatea, V.I. Popa, A.C. Mitelut, M.E. Popa, Polylactic acid/cellulose fibres based composites for food packaging applications, Mater. Plast. 54 (2017) 673–677, https://doi.org/10.37358/mp.17.4.4923.
- [65] E. Sritham, P. Phunsombat, J. Chaishome, Tensile properties of PLA/PBAT blends and PLA fibre-reinforced PBAT composite, MATEC Web Conf. 192 (2018) 1–4, https://doi.org/10.1051/matecconf/201819203014.
- [66] Monika, V. Katiyar, Non-isothermal degradation kinetics of PLA-functionalized gum (fG) biocomposite with dicumyl peroxide (DCP), J. Therm. Anal. Calorim. 138 (2019) 195–210, https://doi.org/10.1007/s10973-019-08231-7.
- [67] N. Makeswaran, D. Das, V. Zade, P. Gaurav, V. Shutthanandan, S. Tan, C. V. Ramana, Size- and phase-controlled nanometer-thick β-Ga2O3 films with green photoluminescence for optoelectronic applications, ACS Appl. Nano Mater. 4 (2021) 3331–3338, https://doi.org/10.1021/acsanm.1c00378.
- [68] D. Das, F.S. Escobar, P.G. Nalam, P. Bhattacharya, C.V. Ramana, Excitation dependent and time resolved photoluminescence of β-Ga2O3, β-(Ga0.955Al0.045) 2O3 and β-(Ga0.91In0.09)2O3 epitaxial layers grown by pulsed laser deposition, J. Lumin. 248 (2022), https://doi.org/10.1016/j.jlumin.2022.118960.

- [69] Z.L. Wang, G. Zhu, Y. Yang, S. Wang, C. Pan, Progress in nanogenerators for portable electronics, Mater. Today 15 (2012) 532–543, https://doi.org/10.1016/ \$1369.7021(13)70011.7
- [70] Z. Wang, X. Pan, Y. He, Y. Hu, H. Gu, Y. Wang, Piezoelectric nanowires in energy harvesting applications, Adv. Mater. Sci. Eng. 2015 (2015), https://doi.org/ 10.1155/2015/165631.
- [71] Y. Zi, Z.L. Wang, Nanogenerators: an emerging technology towards nanoenergy, APL Mater. 5 (2017), https://doi.org/10.1063/1.4977208.
- [72] B. Sun, X. Li, R. Zhao, H. Ji, J. Qiu, N. Zhang, D. He, C. Wang, Electrospun poly (vinylidene fluoride)-zinc oxide hierarchical composite fiber membrane as piezoelectric acoustoelectric nanogenerator, J. Mater. Sci. 54 (2019) 2754–2762, https://doi.org/10.1007/s10853-018-2985-x.
- [73] A.M.M. Roji, G. Jiji, A.B.T. Raj, A retrospect on the role of piezoelectric nanogenerators in the development of the green world, RSC Adv. 7 (2017) 33642–33670, https://doi.org/10.1039/c7ra05256a.
- [74] S.S.H. Abir, M.U.K. Sadaf, S.K. Saha, A. Touhami, K. Lozano, M.J. Uddin, Nanofiber-based substrate for a triboelectric nanogenerator: high-performance flexible energy fiber mats, ACS Appl. Mater. Interfaces 13 (2021) 60401–60412, https://doi.org/10.1021/acsami.1c17964.
- [75] D. Lopez, A.R. Chowdhury, A.M. Abdullah, M.U.K. Sadaf, I. Martinez, B. D. Choudhury, S. Danti, C.J. Ellison, K. Lozano, M.J. Uddin, Polymer Based triboelectric nanogenerator for cost-effective green energy generation and implementation of surface-charge engineering, Energy Technol. 9 (2021) 1–9, https://doi.org/10.1002/ente.202001088.
- [76] L. Zhang, J. Gui, Z. Wu, R. Li, Y. Wang, Z. Gong, X. Zhao, C. Sun, S. Guo, Enhanced performance of piezoelectric nanogenerator based on aligned nanofibers and threedimensional interdigital electrodes, Nano Energy 65 (2019), 103924, https://doi. org/10.1016/j.nanoen.2019.103924.



Sk Shamim Hasan Abir received his B.Sc. in Mechanical Enginering form Bangladesh University of Engineering and Technology in 2017. Then he joined the University of Texas Rio Grande Valley as a graduate student in Mechanical Engieering department in 2019. His research interests include polymer nanocomposite, perovskite nanocrytals, piezo/triboelectric nanogenerator flexible eletronics and biosensors. He was awarded the Presidential Graduate Research Assistantship (2019–2021), Margaret Draper Scholarships (2020) and AT&T-UTPA Scholarships (2021) for his academic performance.



Julio E. Trevino received his mechanical engineering master's ('21) and bachelor's degree ('19) from the University of Texas Rio Grande Valley. He worked, mentored and is a part of the UTRGV Partnership for Research and Education in Materials Science (PREM) team under Dr. Karen Lozano since 2019. He was awarded the prestigious Presidential Graduate Research Assistantship in 2019. His research mainly focuses on renewable energy applications such as thermoelectric and piezoelectric nanofibers and nanogenerators. He is currently working in the air and defense industry as a research scientist.



Dr. Bhupendra B. Srivastava is a lecturer of Chemistry at the University of Texas Rio Grande Valley. He received his BSc and MSc degree from the Banaras Hindu University, India and PhD degree from the Calcutta University, India. His research focuses on designing new (persistent) luminescent materials and nanomaterials via colloidal and hydrothermal synthesis for high-power lighting, imaging and sensing applications. As of today, he has co-authored more than 20 peer-reviewed journal articles.



Muhtasim Ul Karim Sadaf graduated with a BSc in Chemical Engineering and Polymer Science from Shahjalal University of Science and Technology, Bangladesh, in 2018. He then graduated with an MS in Chemistry from the University of Texas Rio Grande Valley (UTRGV) in 2021. He is the recipient of the prestigious Presidential Graduate Research Assistantship, Henry Poppenhagen Endowed Scholarship, Elliot Endowed Departmental Scholarship at UTRGV. He started his Ph.D. in Engineering Science and Mechanics at Penn State from 2021.



Dr. Karen Lozano is a Mechanical Engineering Professor and Founder/Director of the University of Texas Rio Grande Valley (UTRGV) Nanotechnology Center, received her BS from Universidad de Monterrey and MS/PhD from Rice University. She has provided research opportunities to hundreds of UG students. Recipient of several honors such as the US PAESMEM, National Academy of Inventors Fellow, and TEDx Speaker. Lozano's team has published > 165 journal articles and > 500 proceedings/conference presentations. She outreaches to thousands of K-16 students through summer camps, magic/science shows, and social media, all with one goal in mind: preparing future innovators.



Julia I. Salas obtained her B.S. in Civil Mining Engineering, in the University of Talca, Chile in 2020. Later, she obtained her M.S. in Mechanical Engineering in the University of Texas Rio Grande Valley, in 2021. Her research interest mainly are in energy harvesting devices and how to functional polymers for this objective.



Dr. Mohammed Jasim Uddin (Associate Professor) obtained his Ph.D. degree (Materials Science) from University of Turin, Italy and currently holding the position of Director of Photonics and Energy Research Laboratory (PERL) in the Department of Chemistry, University of Texas Rio Grande Valley. He is known for the invention of three-dimensional solar cells, and self-cleaning, antimicrobial textiles, and photochromic textiles. He has an *h-index* of 29 and an i-10 index of 111 with over 4500 citations with 72 papers and 130 referred presentations and is recently awarded: High Scholar Research Competition Award 2016, 2018, & 2020 (UTRGV), Outstanding and Sustainable Research in Science Award 2016 (UTRGV), United Group

Research Award 2016 (International), NASA Texas Space Grant Award (2016), UGC Award in 2010 (International), etc. He received over \$21*M* external research grant award to support his research in advanced *material* science.